Building integration of semitransparent perovskite-based solar cells: Energy performance and visual comfort assessment

Post-print version of the paper published in Applied Energy, Volume 194, 15 May 2017, Pages 94-107, doi: https://doi.org/10.1016/j.apenergy.2017.03.011

Building integration of semitransparent perovskite-based solar cells: Energy performance and visual comfort assessment

Alessandro Cannavale[a,], Maximilian Hörantner[b], Giles E. Eperon[c], Henry J. Snaith[b] , F. Fiorito[d], Ubaldo Ayr[a] and Francesco Martellotta[a]*

a) Politecnico di Bari, DICAR, via Orabona 4, 70125 Bari (Italy)
b) University of Oxford, Clarendon Laboratory, Parks Rd, Oxford, OX1 3PU, United Kingdom
c) Department of Chemistry, University of Washington, Seattle, WA 98105, USA
d) University of Sydney

Abstract

This study presents a simulation of the yearly energy production and visual comfort benefits deriving from the adoption of building integrated semitransparent photovoltaic windows. Measured electrical and optical properties of neutral-colored solid-state planar heterojunction perovskite cells, characterized by promising transparency and photovoltaic conversion efficiency, were applied to a hypothetic photovoltaic glazing. Such experimental data were used as input to estimate annual energy production and visual comfort effects. The effect of different climate conditions was also investigated. A south-oriented test-room was modelled, assuming two window-to-wall ratios of for office buildings, (19%) and (32%), respectively. Energy yield was calculated at different locations showing figures between 20 and 30 kWh/m^2 per year, with negligible reduction (not exceeding 3% in the hottest climates) when cell temperature was taken into account. Visual comfort assessment was carried out using two typical metrics: Useful Daylight Illuminance (UDI) and Daylight Glare Probability (DGP), comparing the performances of a photovoltaic glass with those of a commercial solar control glass and of a clear glass, acting as a reference. We found that that the use of photovoltaic glass, independent of the location latitude, showed a significant increase in UDI values respect to clear glasses and performances comparable to solar control glasses. With reference to DGP, the use of photovoltaic glass allowed to reduce the percentage of work hours with high DGP

Post-print version of the paper published in Applied Energy, Volume 194, 15 May 2017, Pages 94-107, doi: https://doi.org/10.1016/j.apenergy.2017.03.011

between 12% and 23% depending on the location. Finally, we compared the annual energy production of building integrated photovoltaic cells to the annual use of electric energy for artificial lighting, finding that in most of the cases the annual energy production overcomes the amount of electric energy used for artificial lighting.

1 Introduction

According to the agreement of COP21, global warming should be kept below 2 °C by means of a massive reduction of greenhouse gas emissions (GHG). All new buildings will have to be nearly zero energy, as appointed by the European Directive 2012/13/EU, i.e. buildings with very low yearly energy consumption, due to energy efficient design and to the use of renewable energy sources. [1]

In this roadmap, a strong effort to the effective exploitation of innovative renewable sources (e.g. photovoltaics (PV), wind energy, etc.) could bring manifold advantages: firstly, the attenuation of foreign dependence but also a stimulus to a sustainable approach to development. Nowadays, PVs can be considered an established technology that can contribute significantly to lower GHG emissions and energy consumption in new buildings as well as in existing ones.

Building Integration of Photovoltaics (BIPV) is recognized worldwide as a relevant chance to integrate PV elements in the design of building components: BIPV has been identified as a suitable technology to improve building energy consumption performances and to reduce their ecological footprint. BIPV is a better alternative to Building Adopted PV (BAPV) systems, where PV panels are simply attached on exterior parts of building envelopes (on rooftops or facades). BIPV systems represent architecturally relevant components, active energy-producing units requiring the complex fulfillment of multiple requirements (aesthetic, economic, structural, acoustic, thermal, etc.). [2,3]

PV modules based on crystalline silicon cells (c-Si), still predominant on the market (with conversion efficiencies of 15% for polycrystalline and 20% for monocrystalline silicon cells), [4] are mostly rigid, opaque and flat. Such cells are not suitable for any integration requiring high transparency, even though several attempts have been made to encapsulate c-Si cells in laminated glasses, by adopting a matrix of small panels with transparent

spacing in between. [5,6] Despite this technology being difficult to integrate onto the architectural envelope, it is still one of the preferred solutions, for several reasons: lower costs, a consistent, long-lived mass production and, probably, the misleading consideration that c-Si cells outperform any innovative PV technologies in terms of efficiency, which is not always valid, e.g. in overcast sky conditions and when panels are installed on vertical facades. However, in many emerging technologies, high temperatures or sub-optimal tilt angles which reduce the efficiency of c-Si cells are less significant, ensuring good performances even when poorly irradiated or partially shaded. [5]

These considerations in favor of innovative PV technologies can be even strongly supported by the fact that integration of PV modules into transparent components may be a much more effective choice, particularly in buildings with curtain-wall facades or large skylights. Clearly, in order to avoid affecting the occupants' visual comfort too much, good transparency (or, at least, semi-transparency) becomes a fundamental requirement to comply with. In the last decades, a number of pioneering research investigations dealing with new PV materials has paved the way to the development of semitransparent, color-tunable, flexible, lightweight, robust and easily-processable PV technologies.

Among them, amorphous silicon solar cells (a-Si) [7] have currently reached the best laboratory efficiency of 10.2%. [8] This technology takes advantage of a much lower consumption of silicon with respect to first generation PVs, a lighter substrate (glass), a consolidated industrial process, based on plasma-enhanced chemical vapor deposition (PECVD) and, above all, its range of applications is widened by its peculiar semitransparency. Low-cost, lightweight and flexible a-si:H semitransparent solar cells (η= 3% and T_{vis}= 40%) have already been reported. [1]

A tunable bandgap can be obtained in chalcopyrite-based solar cells, conventionally prepared by subsequent physical vapor deposition (PVD) processes. For example, 2 μm thick Cu(In,Ga)Se_2 (CIGS) solar cells have reached 20% conversion efficiency demonstrating a reliable and promising approach. In order to design semitransparent PV glazings, 1.2 μm thick CIGS solar cells were reported, with a conversion efficiency of 5.6%. [9]

Post-print version of the paper published in Applied Energy, Volume 194, 15 May 2017, Pages 94-107, doi: https://doi.org/10.1016/j.apenergy.2017.03.011

Organic PVs, which use thin, flexible layers of organic light-harvesting molecules to generate power, represent an interesting technology for BIPV, since efficiencies close to the best reported (11.5% can be attained for semi-transparent devices. Nevertheless, their commercial use is still impeded by durability concerns. [10,11]

Photoelectrochemical cells, based on mesoporous, semiconductive photoanodes and electrolytes containing suitably chosen redox couples (e.g. I_3^-/I^-, Br_3^-/Br^-) were named dye sensitized cells (DSCs). [12] They have been considered, for a long time, as a promising technology for their possible use as an inherently semitransparent PV technology. Nevertheless, chemical degradation, leakage problems due to the use of liquid electrolytes, photochemical degradation of dyes and sealants still act as limiting factors affecting the reliability of this technology.

More recently, the emergence of perovskite-based solar cells has revolutionized the field of new generation PVs. They are easily-processable, solid-state high conversion efficiency solar cells, [13] most commonly based on hybrid organic-inorganic metal halides (ABX_3), with A = (CH_3NH_3, NH_2CHNH_2, Cs), B = (Pb, Sn) and X= Br, Cl, I enabling accurate tuning of bandgaps between ~1.2 and 3eV.[14–16]

A conversion efficiency of 20.1±0.4% has been achieved by this recently developed technology. [8] Several strategies have been proposed in order to realize highly transparent perovskite cells. A typical device consists of a perovskite layer sandwiched between electron and hole transporting materials, respectively in contact with anode and cathode. The perovskite is typically thick enough to absorb all incident light, rendering the device completely opaque. This technology has already been integrated in multifunctional photovoltaic/chromogenic devices. [17] Two main approaches have been reported to enhance cells transparency: making perovskite layers thinner, even if it leads to obtain brownish cells [18] or controlling the perovskite morphology, as to fabricate discontinuous micro-islands by tuning the physical parameters of the perovskite deposition process. [19] Such islands, when suitably designed, are invisible to the naked eye and form neutral-tinted films, with minimal impacts on the spectral properties of light entering indoor. Recently, since such perovskite films with reduced coverage suffer from the contact between hole and electron transporting layers, which provides lower resistance (shunt) pathways, Hörantner et al. [20] improved this method by blocking these

Post-print version of the paper published in Applied Energy, Volume 194, 15 May 2017, Pages 94-107, doi: https://doi.org/10.1016/j.apenergy.2017.03.011

"shunting paths" via deposition of transparent, insulating molecular layers, via the use of an insulating octadecyl-siloxane molecular layer. This layer preferentially attaches to the exposed areas of electron transporting TiO_2, without obstructing the charge transport through the perovskite.

As it is quite predictable, BIPV not only affects energy aspects of the entire annual building energy balance, but also influences visual comfort concerns when it is applied to windows and other similar elements. According to Boyce et al., [21] the minimum acceptable glazing transmittance, in modern offices, lies in the range between 25% and 38%. This means that solar cells encapsulated in laminated glasses should overcome a threshold value in average transmittance for being considered suitable envelope technologies. Zomer et al. [22] investigated the balance between aesthetics and performance in building integrated first generation photovoltaics. Yang and Zou [23] investigated benefits and barriers to the diffusion of BIPV technologies. The manifold advantages and potentialities of BIPV technology were thoroughly investigated, such as the reduction of carbon emissions and social costs, environmental impact of constructions, significant reduction in land use for the generation of electricity and savings on electricity bills. They also highlighted that BIPV systems may result in a mere cost offset by replacing traditional building materials in architectural envelopes. As reported by Benemann et al. [6], compared to a standard glass facade or a structural glazing facade, BIPV of silicon cells means additional cost of about 350-500 $/m^2. More recently, Chae et al. [24] suggested a procedure to evaluate the energy performance of buildings incorporating BIPVs, considering not only the electrical characteristics of PV cells, but also thermal and optical behavior and the consequent implications on building energy performance. They found that the maximum electric energy generation using a-Si:H cells could range from 22 kWh/m^2 per year to 45 kWh/m^2 per year, depending on several parameters including the type of PV cell, the site location and the exposition. Oliver et al. [25] studied the influence of building integrated semitransparent solar cells (BISTSC) on heating, cooling and lighting loads and electricity generation, considering parameters like Window-to-wall-ratio (WWR) and cells average transmittance (T_{vis}). They found that a BISTSC on larger windows (WWR>33%) could provide a promising energy saving potential between 18% (WWR=33%) and 59% (WWR=88%), compared to regular glass. In this work, we adopted a parametric approach, considering relevant

Post-print version of the paper published in Applied Energy, Volume 194, 15 May 2017, Pages 94-107, doi: https://doi.org/10.1016/j.apenergy.2017.03.011

figures of merit to determine ideal geometric configuration of building integrated semitransparent perovskite films. Some of the authors already used a similar approach to assess the benefits deriving from building integration of photoelectrochromic technologies. [26–28]

This study aims to demonstrate that the reported perovskite-based PV technology offers two advantages if integrated into buildings. In fact, it not only produces an annual amount of electric energy which is comparable to that obtained by using commercial a-Si cells, but also can be exploited as solar control films for glasses, effectively shielding undesired solar gains and thus allowing energy saving and the achievement of higher levels of visual comfort indoors.

Different values of WWR, different site locations and visual transmittance (T_{vis}) of different glasses (clear glasses, solar control glasses and perovskite glasses) and PV parameters deriving from experimental measurement of neutral-colored highly transparent perovskite solar cells were considered (fill factor, open-circuit voltage, short-circuit current and conversion efficiency). The electro-optical features of these cells were utilized as an input for our simulation activities, in order to figure out several effects deriving from their potential adoption on building facades. To this aim, specific tools were adopted, allowing an assessment of potential yearly electric energy production (Matlab) as well as the implications on visual comfort (Daysim).

2 Methods

In this multidisciplinary study, we decided to adopt the principle of "design driven research", commonly used in the field of facade engineering design. We combine the experimental activities of production and characterization of highly transparent perovskite based photovoltaic cells with simulations of annual energy production as well as natural light penetration in a standard test room with transparent surfaces equipped with these innovative, neutral-colored films.

Such an approach is based on the basic consideration that the experimental and simulation activities are characterized by different parameters mutually influencing each other. For this reason, we opted to use the output of the experimental activity (colorimetric and

electro-optical characterization of solar cells) as an input for the simulation tests reported hereafter. This approach allows to achieve important feedbacks for a re-design activity, taking into account geometric, typological, comfort, regulations and climate constraints, not predictable in the laboratory activity.

All the bibliographic references available dealing with these kind of devices concern laboratory scale devices. [19,20] No scale-up or development activities have been demonstrated. So, a preliminary study as proposed in this paper can contribute to improve the design quality at the early stage of technology development. A similar approach has been used to predict the efficacy of building integration strategies of small-area devices not already scaled up in the case of electrochromic devices, recently, by De Forest et al. [29–31] The pivotal parameters chosen for driving the design of the new devices were the annual energy production by photovoltaic conversion and visual comfort assessment of indoor spaces.

2.1 Semi-transparent solar cells fabrication and electro-optical characterization

The neutral coloured semi-transparent perovskite solar cell devices were prepared for this study according to the method described by Hörantner et al. [20]

In summary the procedure involved the rigorous cleaning and patterning of FTO/glass substrates, the subsequent coating of a compact TiO_2 n-type layer and the deposition of dewetted perovskite islands. Shunt-blocking layers from Octadecyl-trichloro silane were additionally applied to improve the device performance before the hole transporting layer spiro-OMeTAD was deposited. A flexible Nickel micro grid was laminated to act as a transparent hole conducting electrode.

The measurement of the performance of the solar cells was carried out under simulated AM 1.5 sunlight, generated with a class AAB ABET solar simulator. For one sun intensity it was calibrated to give simulated AM 1.5, of 100 $mWcm^{-2}$ equivalent irradiance, using an NREL-calibrated KG5 filtered silicon reference cell. Neutral density filters were used to reduce the intensity of the simulated sun light and the mismatch factor was calculated to obtain the corrected performance. The current-voltage curves were recorded with a sourcemeter (Keithley 2400, USA). The solar cells were masked with a metal aperture defining the active area (0.0929 cm^2 or 0.71 cm^2) of the solar cells.

Post-print version of the paper published in Applied Energy, Volume 194, 15 May 2017, Pages 94-107, doi: https://doi.org/10.1016/j.apenergy.2017.03.011

The performances of these cells, which were adopted at the basis of the reported simulations, were summarized in Table 1.

Table 1 – Photovoltaic and optical parameters of highly transparent perovskite solar cells.

Light intensity W/m2	*Current density (Jsc) mA/cm2*	*Fill factor (FF)*	*Open circuit voltage (Voc) V*	*Conversion efficiency (η) %*	*Maximum Power Point Voltage V*	*Average Visual transmittance %*
1000	11.03	0.65	0.9532	6.64	0.68	42.4

Spectral transmittance measurements were carried out with an internally coupled integrated sphere in a Varian Cary 300 UV-visible spectrophotometer. Starting from data measured in laboratory cells, visual transmittance was calculated according to the European Standard EN410, which specifies methods of determining the luminous and solar characteristics of glazing in buildings. The total transmittance spectrum of the semi-transparent solar cell that was used for this simulation is shown in Figure 1.

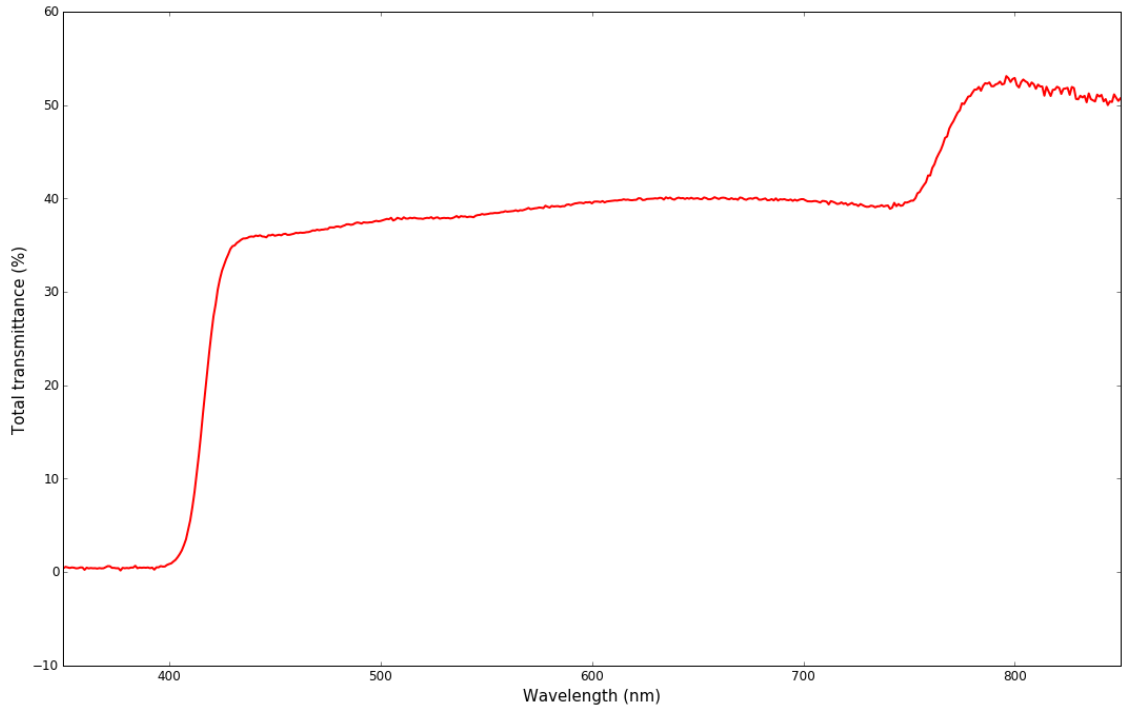

Figure 1: Total transmittance spectrum of semi-transparent solar cell, measured with UV-vis spectrometer.

The CIE 1931 color space was used to obtain the color perception of the human eye by calculating the tristimulus values, which relate to the spectral response of the cone cells

Post-print version of the paper published in Applied Energy, Volume 194, 15 May 2017, Pages 94-107, doi: https://doi.org/10.1016/j.apenergy.2017.03.011

within the human eye. These values can be found by integrating the product of the sun's irradiance spectrum transmitted through the solar cell and the individual standardized CIE color matching functions ($\bar{x}$, $\bar{y}$, $\bar{z}$) over the visible spectrum of the eye:

$$X = \int_{380\ nm}^{780\ nm} I_{sun}(\lambda)T(\lambda)\bar{x}(\lambda)d\lambda$$

$$Y = \int_{380\ nm}^{780\ nm} I_{sun}(\lambda)T(\lambda)\bar{y}(\lambda)d\lambda$$

$$Z = \int_{380\ nm}^{780\ nm} I_{sun}(\lambda)T(\lambda)\bar{z}(\lambda)d\lambda$$

The tristimulus values are then used to calculate the x, y color coordinates on the chromaticity diagram, which is shown in Figure 2 and demonstrates how we would perceive the color.

$$x = \frac{X}{X+Y+Z}$$

$$y = \frac{Y}{X+Y+Z}$$

Under standard conditions it is assumed that the sun's intensity is equal to the AM1.5 solar spectrum, which lies very central (perceived as neutral color) within the chromaticity diagram with coordinates of x = 0.332 and y = 0.343 and as we obtained an almost constant transmittance over the visible spectrum (see Figure 1), the color coordinates have not changed much (x = 0.333 and y = 0.342) so that the color perception of light transmitted through the solar cell can be described as neutral in this work.

Post-print version of the paper published in Applied Energy, Volume 194, 15 May 2017, Pages 94-107, doi: https://doi.org/10.1016/j.apenergy.2017.03.011

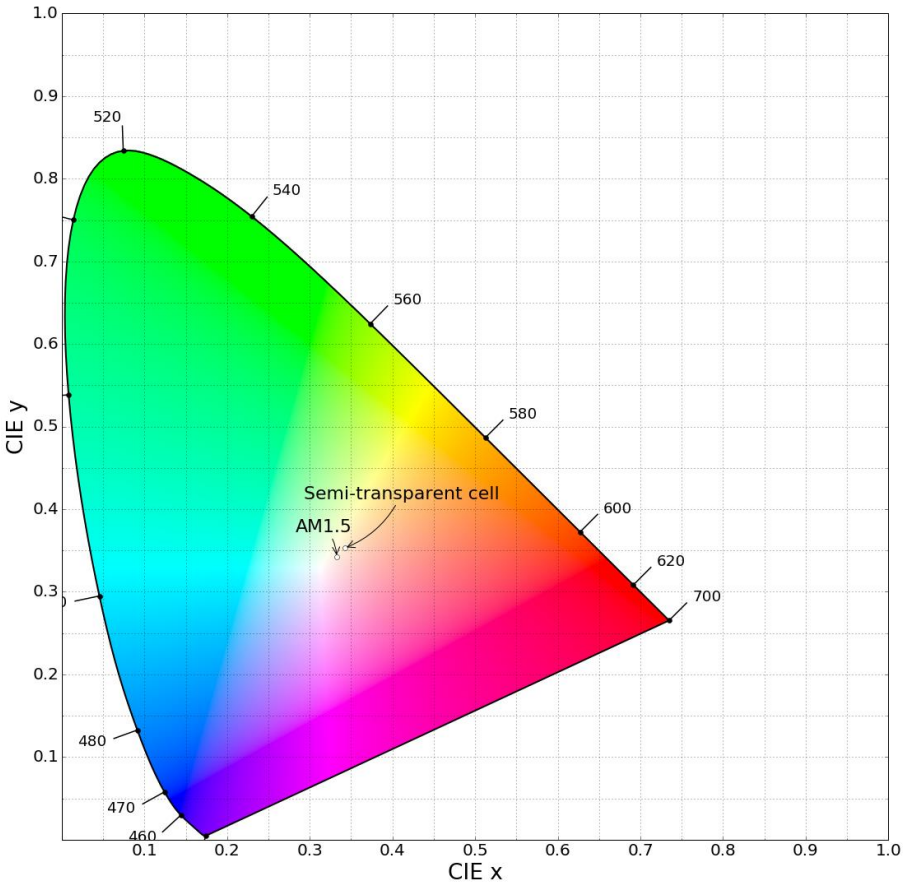

Figure 2: CIE 1931 chromaticity diagram with color perception of AM1.5 spectrum and spectrum transmitted through semi-transparent solar cell.

2.2 Estimation of Annual energy production

The analysis was carried out by taking into account actual (experimental) efficiency of the cell as a function of radiation intensity. Considering the reasonably linear behavior (Figure 2), a simple regression model was used to derive efficiency at each specific value of impinging radiation intensity.

Radiation intensity values for the simulation were retrieved for different locations from IWEC (International Weather for Energy Calculations) database developed by ASHRAE within the Research Project RP-1015, [32] and made available through the EnergyPlus website. This dataset provides hourly values of the most important weather data, together with the overall radiation calculated using an empirical model based on the sun-earth geometry, reported cloud cover, temperature difference from three hours previously, relative humidity, and wind speed for 227 locations outside USA and Canada. Normal

Post-print version of the paper published in Applied Energy, Volume 194, 15 May 2017, Pages 94-107, doi: https://doi.org/10.1016/j.apenergy.2017.03.011

solar radiation is provided as a function of the solar angle and the ratio of the derived total global horizontal compared to the extraterrestrial solar radiation. In this way, using data belonging to the same set, a consistent evaluation was carried out among the different locations. In addition, this dataset is available through the widespread used EnergyPlus platform [33], which is becoming the "de facto" standard for energy calculations in buildings. Then, in order to combine the hourly values of direct and diffuse radiation with the cell efficiency the sun path trajectory was calculated for each location using a script developed in Matlab and based on well known astronomical relations. Diffuse radiation was calculated using two different methods. In the first case a simple isotropic sky model was used, according to which the diffuse radiation is uniform across the sky, and the consequent amount impinging on the cell surface can be obtained by multiplying by the view factor (given by $(1+\cos \beta)/2$, with β being the tilt angle). The second model was the anisotropic model developed by Perez et al. [34] , according to which diffuse radiation is split among three different components accounting for the horizon, circumsolar, and isotropic (dome) radiation. All the variables required for the correct application of the method can be retrieved from the weather data file. Calculations were performed using the same updated brightening coefficients used in EnergyPlus.

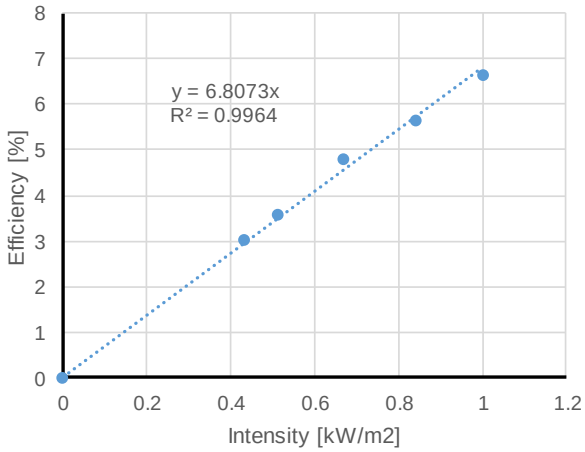

Figure 2. Plot of efficiency of Perovskite semi-transparent PV cell vs. solar radiation intensity.

As at this stage the purpose is mostly that of analyzing the cell performance under different climatic conditions, the effect of inverters, charge controllers, batteries, or

maximum power point trackers was not included in the calculation and the whole electrical part was supposed to operate under ideal conditions. Thus the resulting values should be intended as the upper limit of electricity production. However, as the cell temperature may be significantly influenced by climatic conditions, and for the cell under investigation a 0.3% decrease was measured per each Celsius degree in excess of STC temperature, this effect was taken into account following the procedure described in the Appendix. The efficiency decrease was measured in laboratory tests.

In all the cases the cell was assumed to be on a vertical unobstructed surface facing South (North for locations in the Southern hemisphere), with no extra radiation due to reflections and to ground.

The locations were chosen so to compare different latitudes (in both Southern and Northern hemisphere) and have at least two different climatic conditions derived from the Koppen-Geiger classification system [35]. For more information about the locations adopted, see Table 2.

Table 2. Summary of geographic and meteorological characteristics of the selected locations, together with the yearly average temperature and rainfall (source climate-data.org), the average sky cover and overall radiation on horizontal surface (source IWEC dataset).

City	*Lat. [°]*	*Koppen-Geiger Climate Class*		*Avg. Temp. [°C]*	*Avg. Rainfall [mm]*	*Avg. Sky Cover [0-10]*	*Horiz. Radiation [kWh/m^2.yr]*
Reykjavik	64.13	Subarctic	Dfc	4.7	869	7.7	753
Bergen	60.30	Temperate oceanic	Cfb	6.8	2251	7.2	738
Moscow	55.75	Humid continental	Dfb	4.9	679	7.0	966
Berlin	52.47	Warm humid continental	Dfb	9.1	570	6.1	980
London	51.15	Temperate oceanic	Cfb	11.1	621	6.7	1001
Brindisi	40.65	Warm mediterranean	Csa	16.5	598	4.7	1569
Thessaloniki	40.52	Cold semi arid	Bsk	15.9	445	4.3	1497
Aswan	23.97	Hot desert	Bwh	26.8	1	0.9	2294
Guangzhou	23.13	Humid subtropical	Cfa	22.2	1720	7.0	1067
Dakar	14.73	Warm semi-arid	Bsh	24.9	469	4.4	1926
Manila	14.52	Tropical savanna	Aw	23.7	2047	6.2	1566
Sydney	-33.95	Humid subtropical	Cfa	17.6	1309	4.9	1645
Cape Town	-33.98	Warm summer medit.	Csb	16.9	853	3.9	1829

2.3 Daylighting metrics - Test room settings and simulation parameters

Simulations reported in this study were carried out by modelling a test room using Daysim, a validated Radiance-based program, able to predict indoor annual luminance

and illuminance levels under real-sky conditions derived from statistical weather files. [36] The tool combines a backward-ray-tracing algorithm with the daylight coefficient approach. [37] In the Daysim model all the opaque materials have been simulated using the Radiance plastic function, while the transparent materials (both photovoltaic and clear glass) have been simulated through the glass algorithm. More in detail, Radiance-based calculations simulate glass as a special dielectric, accounting for the angular dependence of visual and solar transmission. The general algorithm takes into account the material's refraction, usually set at 1.52, the incidence angle of solar radiation, and the inter-reflections between the two surfaces of the panel. Thus, the only input variable is the transmissivity, typically used in radiance-based simulations, which is related to the visual transmittance as reported in [38].

Two comfort parameters chosen for assessing the feasibility of BISTSCs as a transparent material for windows are UDI and DGP. Useful Daylight Illuminance (UDI) parameter, developed by Nabil et al. [39,40], considers absolute daylight illuminance levels calculated on hourly-based meteorological data collected over a period of a full year.

Then, Useful Daylight Illuminances are defined as percentages of time in which the illuminances of sensors fall within a range of values considered comfortable by the users. According to previous literature reviews on occupants' preferences and behaviors [39], a range of 100–2000 lux has been considered suitable for the current project. In place of a threshold value, UDI proposed a range of illuminances that represent useful levels of illumination, which providing a more informative metric respect to a simple threshold metric level. Daylight illuminances less than 100 lx are generally considered insufficient, whereas daylight illuminances higher than 2000 lx are likely to produce visual or thermal discomfort. Consequently, UDI is defined as the percentage of time in which the daylight illuminances fall within the selected range. On the other hand, glare stands among the critical factors affecting the level of visual comfort in daylit office spaces. For this reason, Daylight Glare Probability (DGP) was developed by Wienold and Christoffersen who found [41], using a random optimization method, a strong correlation between the probability of perceived discomfort and a combination of vertical eye illuminance and the ratio of the luminance of direct and indirect sources to the adaptation term (which is again depending on the vertical illuminance). DGP is a glare parameter which proved to predict the discomfort due to excess glare, taking into account not only the luminance gradient

Post-print version of the paper published in Applied Energy, Volume 194, 15 May 2017, Pages 94-107, doi: https://doi.org/10.1016/j.apenergy.2017.03.011

within the visual field but also the total vertical eye illuminance for a viewing hemisphere of 2π sr. It quantifies the probability of the occurrence of glare due to direct solar radiation and/or high contrast in the field of view.

DGP is a function of the vertical eye illuminance as well as of the glare source luminance, its solid angle and its position index. For the calculation of DGP Eq. (1) was used, which is already described in the most recent literature in the field [41]:

$$\mathrm{DGP} = 5.87 \times 10^{-5} E_V + 9.18 \times 10^{-2} \log\left(1 + \sum_i \frac{L_{s,i}^2 \omega_{s,i}}{E_V^{1.87} P_i^2}\right) + 0.16 \quad (1)$$

where E_v is the total vertical eye illuminance, while L_s, ω_s and P are respectively the luminance, solid angle and weight factor for each of the n glare sources i.

According to Mardaljevic et al. [42], three classes of environment can be defined according to the value of DGP: ‘‘imperceptible” glare (DGP < 0.35 for 95% of the occupied time); ‘‘perceptible” glare (DGP < 0.40 for 95% of the occupied time); ‘‘disturbing” (DGP < 0.45 for 95% of the occupied time). Such ranges were defined asking subjects to perform different tasks (e.g. reading a paper, working on a computer) and collecting users’ performances, like the number of errors or speed at performing each task. [41] Subjects involved were asked to associate the magnitude of glare on a scale showing four glare levels (imperceptible, noticeable, disturbing and intolerable) and whether they would rate the lighting condition suitable for a work place.

In this work, DGP values have been calculated using the Daysim algorithm. The modelled test room has an indoor rectangular area of 20 m^2 (4 m × 5 m), with a net height of 3.5 m in order to model a typical room within an office building (Figure 3). The modeled rooms have single openings on one smaller side: a smaller window of 2.6 m^2 area, equivalent to 13% of floor area and a window to wall ratio WWR of 19% in respect to the south wall area; a larger strip window of 4.5 m^2 area (22% of floor area and a WWR of 32% calculated on south wall area). In this way, we simulated typical daylighting penetration conditions in office buildings.

Post-print version of the paper published in Applied Energy, Volume 194, 15 May 2017, Pages 94-107, doi: https://doi.org/10.1016/j.apenergy.2017.03.011

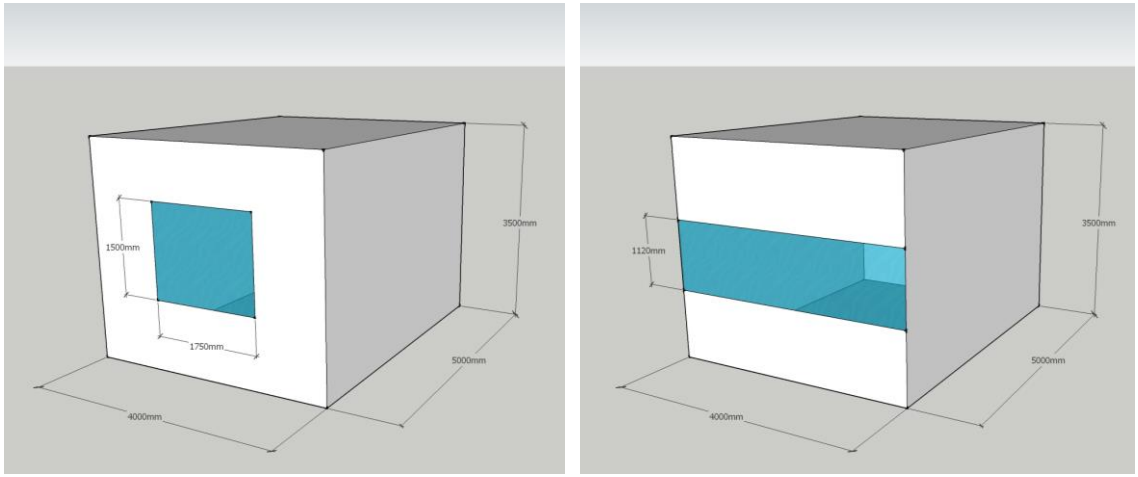

Figure 3 – View of the two room models

We set up a reference grid of illuminance sensors, made of 12 surveying points and set up at 85 cm above the floor level, corresponding to the ideal height of a workplane. To avoid edge effects due to the proximity of indoor and outdoor walls, the reference grid was spaced out of 1 m from each border. The view point was placed in the middle of the room at a distance of 2 m from the window and at a height of 1.1 m above the floor level, thus representing the position of a typical seated user. In order to maximize the glare phenomenon, the viewpoint was oriented towards the corner with the highest luminance gradient. As requested by the procedure for the calculation of DGP a view angle of 180° was considered (corresponding to a fisheye camera).

The UDI and DGP analyses were carried out choosing as reference sites the cities of London, Great Britain, (latitude 51°30' N longitude 0°08' W) for its typical Southern British ocean climate, Brindisi, Italy (latitude 40°39' N, longitude 17°57' E), for its typical Mediterranean climatic conditions and Aswan, Egypt (latitude 24°5' N, longitude 32°53' E) with a hot desert climate.

Statistical weather files were used as input for all the simulations, from U.S. Department of Energy, EnergyPlus Energy Simulation software – Weather Data. All the data obtained as output from the simulation process depended on WWR, weather and orientation. South orientation was chosen in order to assess the most critical conditions both in terms of solar control utilization of glasses and in terms of annual energy production.

Post-print version of the paper published in Applied Energy, Volume 194, 15 May 2017, Pages 94-107, doi: https://doi.org/10.1016/j.apenergy.2017.03.011

All the analyses were carried out for an entire year (derived from the weather file as statistically significant), selecting the working hours. In detail, two time slots have been selected: the morning one between 8.00 am and 5 PM for the weekdays (Monday to Friday). As the general aim of indoor natural illuminance levels calculations was to compare photovoltaic windows with traditional clear ones, standard material properties included in Table 3 were adopted for the intrados of building fabric (indoor flooring, internal walls, indoor ceiling and transparent surfaces).

As visible in Table 3, three kinds of glasses were adopted in the analyses: a clear glass (CG), acting as a reference, a commercial solar control (SC) glass (the natural colored ANTELIO-SCG was selected) and the perovskite-based photovoltaic (PV) glass at the basis of this study. In such a way, the visual comfort effect of photovoltaic glasses could be compared to common glasses and to solar control glasses already on market.

Table 3 – Material properties

Material	*Colour*	*Reflectance [%]*	*Transmittance [%]*	*Specularity [%]*	*Roughness [%]*
Indoor flooring	Stone grey	45.54	0.00	0.70	1.00
Internal walls	Beige 2k208	65.90	0.00	0.00	0.00
Indoor ceiling	White	85.77	0.00	0.00	0.00
Clear glass	Neutral	-	85.00	-	-
Saint-Gobain glass	Neutral	-	46.00	-	-
PV Pero-glass	Neutral	-	42.40	-	-

In Table 4, the key parameters used in the radiance-based simulations are summarized. The ambient bounces parameter has been set at 5, in order to increase the precision of illuminance calculations and to take into account also multiple reflections on indoor surfaces. [43] The ambient accuracy and ambient resolution parameters were set respectively at 0.1 and 300, in order to obtain, with a maximum scene dimension of 30 m, a minimum spatial resolution of 1 cm. Daysim software also allowed to estimate the annual use of electric energy for artificial lighting and the energy consumption related, expressed in kWh/year.

Table 4 – Set of parameters used for all radiance-based simulations.

Ambient bounces	*Ambient division*	*Ambient super-sample*	*Ambient resolution*	*Ambient accuracy*	*Specular threshold*	*Direct sampling*	*Direct relays*
5	1000	20	300	0.10	0.15	0.20	2

Post-print version of the paper published in Applied Energy, Volume 194, 15 May 2017, Pages 94-107, doi: https://doi.org/10.1016/j.apenergy.2017.03.011

In the standard room, previously described, the user illuminance requirement was considered to be 500 lx (minimum illuminance level) with an installed power density of 12 W/m^2 (according to ASHRAE regulations regarding offices). The lighting control was assumed as a photosensor controlled by dimming system. A loss factor of 15 for fluorescent lamps was taken into account.

3 Results

3.1 Yearly energy production

Following the previously mentioned methodology, for each of the selected locations the resulting values of electric productivity per square meter were given in Table 5, together with the horizontal global radiation, as a reference. As it can be observed, and confirmed by Figure 4, the cells performed best at latitudes between 20° and 45° (in both hemispheres) as a good compromise between the angle formed between Sun and cell (which improves at high latitudes) and radiation intensity (which is at a maximum at the Tropics). Sky coverage and rainfall also played a significant role in changing the electricity yield, as can be seen comparing information in Tables 2 and 5.

Table 5. Summary of yearly electricity production per square meter, calculated according to the different models, for the selected locations.

City	*Lat. [°]*	*Horiz. Radiation [kWh/m^2.yr]*	*Electr. Yield (ISO) [kWh/m^2.yr]*	*Electr. Yield (Perez) [kWh/m^2.yr]*	*Electrical yield (Perez) incl. Temperature effect [kWh/m^2.yr]*
Reykjavik	64.13	753	11.9	16.1	16.1
Bergen	60.30	738	8.7	11.5	11.5
Moscow	55.75	966	13.8	17.7	17.6
Berlin	52.47	980	13.7	17.3	17.1
London	51.15	1001	14.9	18.6	18.4
Brindisi	40.65	1569	23.7	29.4	28.8
Thessaloniki	40.52	1497	22.9	28.2	27.7
Aswan	23.97	2294	28.1	32.9	32.0
Guangzhou	23.13	1067	11.8	13.1	12.8
Dakar	14.73	1926	15.8	18.7	18.2
Manila	14.52	1566	10.5	9.2	9.0
Sydney	-33.95	1645	22.8	27.0	26.4
Cape Town	-33.98	1829	24.9	30.1	29.4

Post-print version of the paper published in Applied Energy, Volume 194, 15 May 2017, Pages 94-107, doi: https://doi.org/10.1016/j.apenergy.2017.03.011

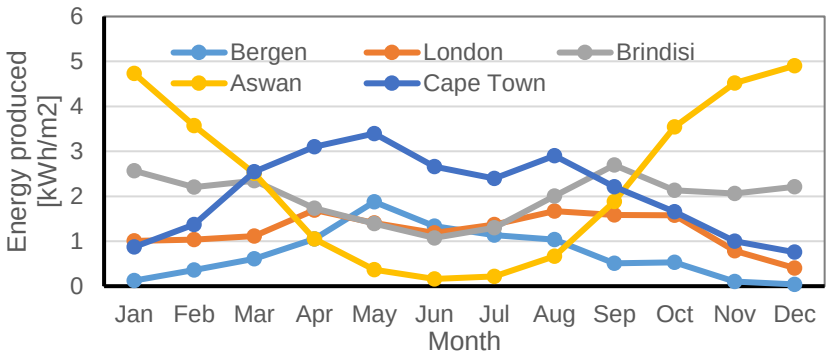

Figure 4. Plot of monthly energy production per square meter of window.

A seasonal dependence also appeared as a function of the latitude. In fact, at northern latitudes Summer was the best season due to lower sky coverage. Conversely, within the temperate belts energy production was at a maximum in Winter because of the most favorable angle and may vary significantly as a function of rainfall. In fact, in Aswan the maximum daily radiation was lower compared to Brindisi, but the radiation pattern was much more uniform because of the very dry climate.

When the cell temperature was taken into account to correct the conversion efficiency, no variations appeared at locations with colder climate, while in the other cases a maximum reduction of 3% was observed in hot desert climates, thus suggesting that transparent PV systems, absorbing less radiative heat than normal opaque systems, were less prone to efficiency reduction due to temperature.

A comparison with the energy performance of other semi-transparent PV windows (or façade solutions) using a-Si cells with similar efficiencies [44,45] shows interesting results. In fact, under Mediterranean climatic conditions [44] the yearly energy output is twice the value observed at locations with similar characteristics. This improved performance is likely due to the efficiency being substantially independent of irradiance intensity for a-Si cells [46]. In fact, even in the Hong Kong study [46] the resulting yearly productivity is about twice the value obtained using our data in Guangzhou, which is the closest location. Anyway, it must be underlined that both the a-Si cells considered have substantially lower transparency, having a transmittance in the visible range equal to 0.07 in the first case and 0.153 in the second. Thus, the potential application of such solutions as clear glass (or solar control glass) replacements is considerably limited compared to perovskite-based cells.

Post-print version of the paper published in Applied Energy, Volume 194, 15 May 2017, Pages 94-107, doi: https://doi.org/10.1016/j.apenergy.2017.03.011

3.2 Visual comfort assessment

With reference to a small size window (WWR = 19%) the UDI distribution (Figure 5) showed that in London, using a clear glass, 75% of the receptors had UDI ≥ 50% (and 42% have UDI≥75%, with a maximum value of 80%), with no receptors in the "poor" range (below 25%). When PV glass was used the maximum UDI lowers to 77%, but all the receptors had a UDI≥50% (the minimum being 53%), and again 42% having UDI≥ 75%. Use of solar control film yields resulted nearly identical to PV treatment.

Moving to Brindisi, the CG case yielded 50% of the receptors in the "excellent" range (with a maximum of 93%) and 25% in the "good", with only 8% in the "poor" range (the

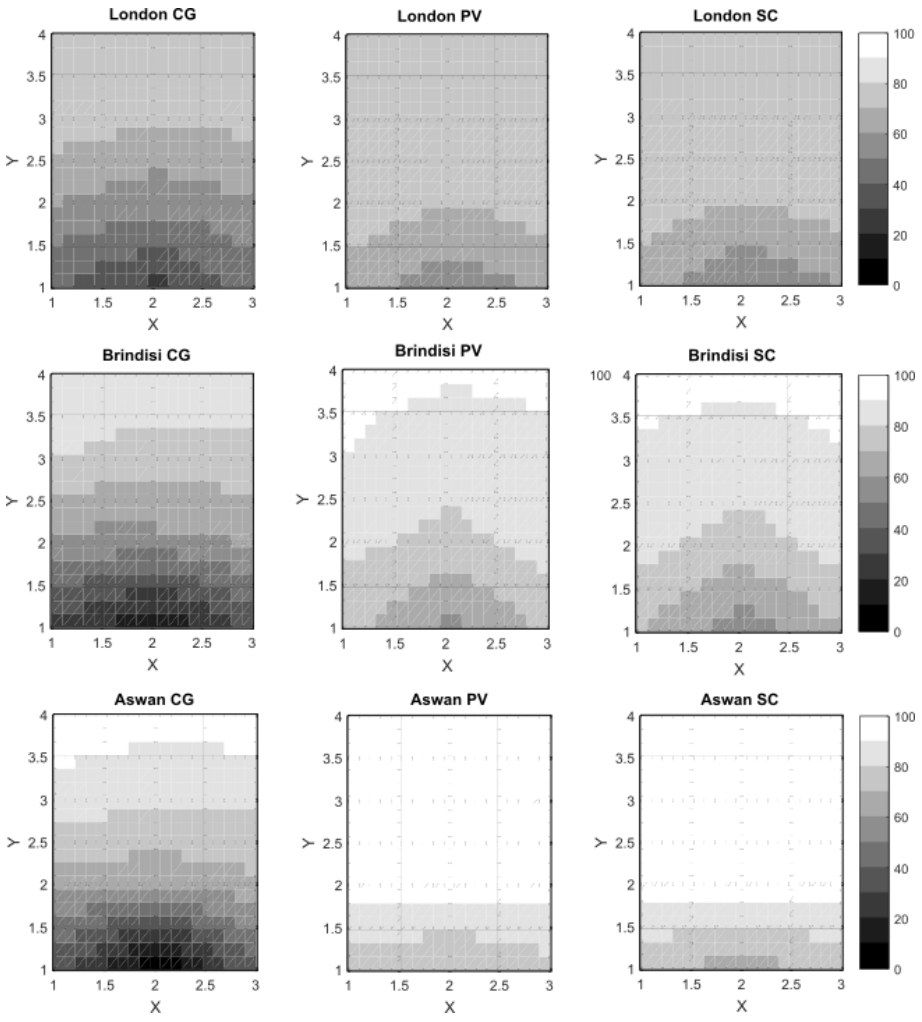

Figure 5 – Spatial distribution of the percentage of time during the work year in which the Useful Daylight Illuminance (UDI) is within comfort limits for the selected locations with a small-size window (WWR = 19%). CG = clear glass; PV = transparent perovskite-based photovoltaic; SC = commercial solar control film. X and Y represent the test-room dimensions, expressed in m.

Post-print version of the paper published in Applied Energy, Volume 194, 15 May 2017, Pages 94-107, doi: https://doi.org/10.1016/j.apenergy.2017.03.011

observed minimum being 13%), for receptors just close to the window. In the PV case a significant improvement took place as the maximum UDI raised to 93% and the minimum to 59%, returning 75% of the receptors in the "excellent" range. In the SC case, results were very similar to PV, with the minimum value decreasing to 55%.

In Aswan, in the CG case UDI spanned over a larger interval, with a maximum of 97% and a minimum of 2% resulting in 50% of the receptors above the 75% limit, 25% above the 50% limit, and 8% below the 25% limit. Use of the PV glass improves significantly the performance, as all the receptors had UDI at least equal to 70% and, in most of the cases, well above. In fact, 92% of the receptors lay in the "excellent" range, and the remaining in the "good". Using the SC film yielded mostly similar results with only a slight decrease in the minimum UDI value.

When the WWR was increased to 32% (Figure 6), more extreme results were observed. In fact, in London, with the CG configuration, UDI varied between 24% and 71%, with no receptors in the "excellent" range, but 50% in the "good" range, and 8% in the "poor" zone. Using PV glass shifted UDI values towards the top, with the overall range spanning between 42% and 79%, and 50% of receptors now having an "excellent" rate, 25% a "good", and no "poor" ratings at all. Use of SC film returned essentially the same results.

In Brindisi the range of variation was extended as UDI spans between 9% and 75%. Only 8% of receptors was in the "excellent" range, and 42% was in the "good" range, while 25% have a "poor" rating, likely as a result of over-illuminance close to the window opening. Use of PV glass made a big impact in UDI as it now spanned between 37% and 95%, with 67% of receptors in the "excellent" range and 8% more in the "good" range, and, obviously, no receptors with "poor" UDI. Use of SC film slightly changed the range of variation (now spanning between 32% and 95%), and the distribution of the values (now having 50% of receptors with "excellent" rating, and 25% with "good" rating).

Finally, in Aswan the range of UDI variation for CG was between 0 and 77%, with the worst conditions observed close to the window opening, in consequence of over-illuminance during the summer months. The UDI values were equally distributed among the four quality classes. Use of the PV glass shifted the values towards to top, as the range

Post-print version of the paper published in Applied Energy, Volume 194, 15 May 2017, Pages 94-107, doi: https://doi.org/10.1016/j.apenergy.2017.03.011

spanned between 48% and 100%, with 75% of the receptors having now an “excellent” rating and 17% a “good” rating. Finally, use of SC film yields similar results, with a range spanning between 43% and 100%, an equal number of “excellent” receptors and an 8% of “good” receptors.

So, at the end of this first group of results, it appeared rather clearly that the use of PV glass offers improved performance compared to standard CG, because, independent of the location latitude, it determined a significant increase in UDI values. In the small-size window case all the receptors had at least a “good” rating, while in the office case a minimum of 75% of the receptors (at the Northern latitudes), had at least a “good” rating, and the percentage increases moving closer to the Tropics. PV glass offered even better performance than commercial SC films, thus confirming its potential on both the energy production and solar control field.

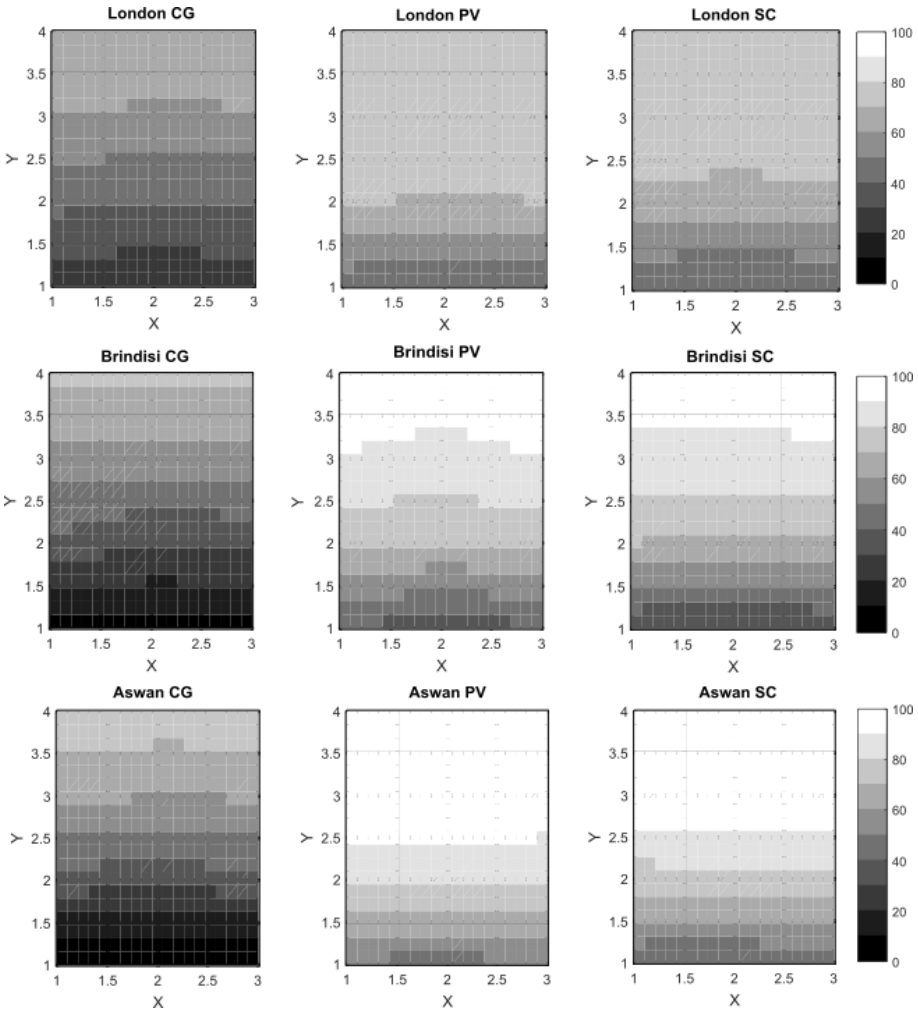

Post-print version of the paper published in Applied Energy, Volume 194, 15 May 2017, Pages 94-107, doi: https://doi.org/10.1016/j.apenergy.2017.03.011

Figure 6 – Spatial distribution of the percentage of time during the year in which the Useful Daylight Illuminance (UDI) is within comfort limits for the selected locations with a typical office window (WWR = 32%). CG = clear glass; PV = transparent perovskite-based photovoltaic; SC = commercial solar control film.

In order to further investigate the advantage resulting from PV glass, its effect on glare reduction was also studied. The same set of data used for UDI analysis was employed to investigate DGP. As explained before, no shading was considered at this stage, in order to allow a comparison with the other options. As shown in Figure 7, as a consequence of the window position on the South wall, the largest variance was observed at hours close to noon, in particular for the smaller window. In fact, the office window allows a larger amount of sun beams to enter the room earlier in the morning and later in the afternoon, thus resulting in a significant amount of scatter in the data (as demonstrated by the larger interquartile range) throughout the whole set of investigated hours. Assuming as a reference a 0.4 DGP value, corresponding to a "good" glare comfort class, for which during 95% of office time glare is weaker than "perceptible" [42] , therefore the following conclusions could be drawn.

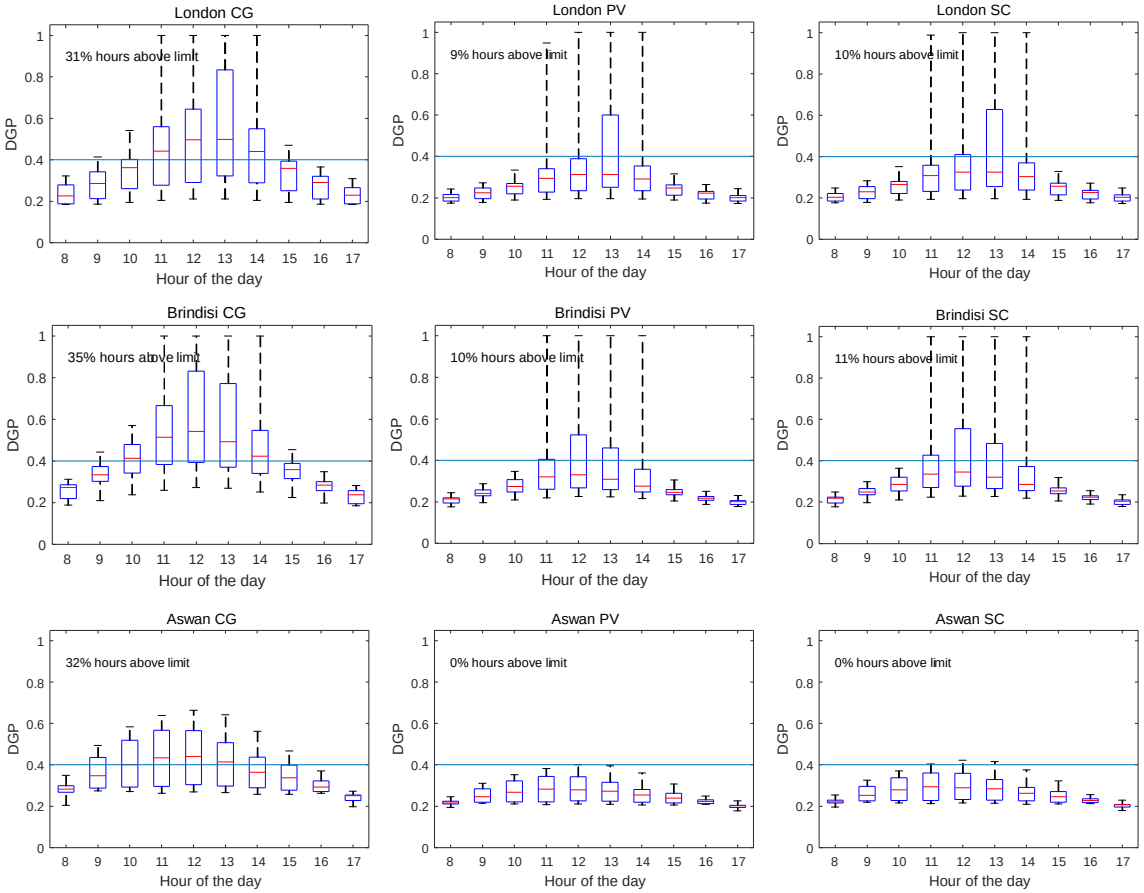

Post-print version of the paper published in Applied Energy, Volume 194, 15 May 2017, Pages 94-107, doi: https://doi.org/10.1016/j.apenergy.2017.03.011

Figure 7 – Boxplot of the Daylight Glare Probability (DGP) yearly distribution for the selected locations as a function of working hours for a small-size window (WWR = 19%). Box represents 1st and 3rd quartiles with the median given by the red horizontal line. Whiskers correspond to minima and maxima in each set. CG = Clear glass; PV = Transparent perovskite-based photovoltaic; SC = commercial solar control film.

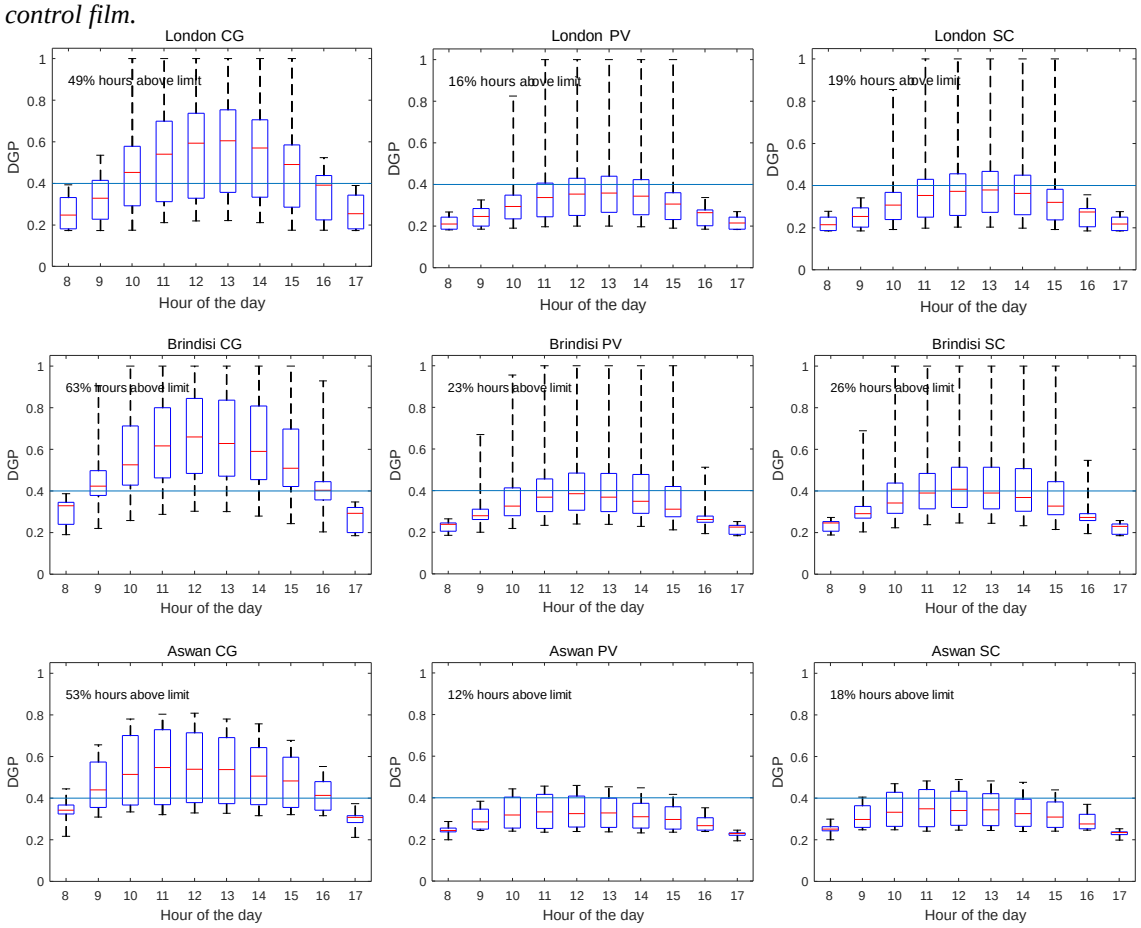

Figure 8 – Boxplot of the Daylight Glare Probability (DGP) yearly distribution for the selected locations as a function of working hours for a typical office window (WWR =32%). Box represents 1st and 3rd quartiles with the median given by the red horizontal line. Whiskers correspond to minima and maxima in each set. CG = Clear glass; PV = Transparent perovskite-based photovoltaic; SC = commercial solar control film.

With reference to the small window (Figure 8) the percentage of work hours of the year in which the limit is exceeded was very similar independent of the location (and the latitude), spanning between 31% in London and 35% in Brindisi. However, the use of PV glass significantly reduced both the median and the interquartile range for all the cases, but the variation was bigger in Aswan, where DGP remains below the limit during all the time, than in the other locations where a residual 10% of work hours exceeding DGP remains. Use of SC film shows similar results. The explanation for this behavior is that at lower latitudes the sun has a smaller zenith angle and, consequently, may penetrate the

Post-print version of the paper published in Applied Energy, Volume 194, 15 May 2017, Pages 94-107, doi: https://doi.org/10.1016/j.apenergy.2017.03.011

room with more difficulty. In fact, the residual percentage in London and Brindisi can be demonstrated to take place when Sun approaches the Winter solstice.

When analyzing the large window, the above behavior was further emphasized. With reference to CG the hours in which DGP is exceeded spanned between 49% for London and 63% for Brindisi, with Aswan standing in between (with a 53% figure). Large interquartile differences appear in all the cases. Use of PV glass allowed to reduce the percentage of work hours with high DGP to 16% in London, 23% in Brindisi and 12% in Aswan. However, high maximum values appeared in the first two cases, while in Aswan maxima laid very close to the 3rd quartile limit. Under such conditions, PV glass outperformed SC film by 3% to 5%, likely because of the better control due to increased transmittance.

Table 6. Use of electric lighting for offices having strip windows with a WWR=32%.

Location	*Type of glazing*	*Annual electric lighting energy load in the test-room [kWh/yr]*	*Annual Electric energy yield (including temperature effect) [kWh/yr]*
	CG	78	-
Brindisi	SC	108	-
	PV	118	129.0
	CG	136	-
London	SC	198	-
	PV	200	82.40
	CG	52	-
Aswan	CG	68	-
	PV	68	143.40

Table 6 reports both the annual electric lighting energy consumption in offices with a strip window (WWR=32%), which showed the highest value of electricity production by photovoltaic conversion. Such windows were equipped with CGs, commercial Saint-Gobain (Antelio) SC glasses and perovskite-based PV films. The yearly electric energy production was also reported for the case of PV windows, taking into account the effect of temperature raise on the PV performances of perovskite-base solar cells. Respect to CGs, either SC or PV films showed a slight increase in annual energy consumption, due to a slightly larger occurrence of low illuminance sensor points (Figure 6). Such increase was more evident in high latitude locations (London), and tends to decrease in Brindisi and, more significantly, in Aswan (low latitude), where all the values were almost

coincident. Moreover, it can be observed that values corresponding to SC glasses and PV glasses are strongly comparable due to the similar values of visual transmittance of the corresponding films. As reported in Table 6, the amount of electric energy produced at Aswan and Brindisi latitudes, 143.4 kWh/yr and 129 kWh/yr, far exceeds the annual electric lighting energy, which were 68 kWh/yr and 118 kWh/yr, respectively. This comparison showed a relevant point: not only were PV glazings able to enhance the comfort and reduce glare in working hours, as shown in the previous paragraphs, but they produce enough energy to offset that used in artificial lighting required for test-rooms.

4 Conclusions

This study reports, for the first time, the potential annual energy production and the visual comfort benefits deriving from the building integration of neutral-colored highly transparent perovskite-based heterojunction solar cells, in architectural glazings. The thermal–optical properties of the BIPV windows were determined from the optical properties of fabricated semi-transparent solar cells. Such data were used as useful input to design test-room models, equipped with photovoltaic, solar control, and reference clear glasses, respectively. Such models were used in the hypothesis of different climatic conditions and WWRs, using Daysim and Matlab softwares.

The results indicated that, for smaller windows, the PV glasses improved the performances respect to clear glasses, as all the receptors had UDI at least equal to 70% and, in most of the cases, well above, showing similar results to SC films. In office test-rooms, using PV glass shifted UDI values towards the top, with the overall range spanning between 42% and 79%, and 50% of receptors now having an “excellent” rate, 25% a “good”, and no “poor” ratings at all. Similar results were obtained with SC films. With reference to DGP, the use of PV glass significantly reduced both the median and the interquartile range for all the cases, in rooms equipped with smaller windows. The variation was bigger in Aswan, where DGP remained below the limit during all the time, than in the other locations where a residual 10% of work hours exceeding DGP remained.

When analyzing the large window, the use of PV glass allowed to reduce the percentage of work hours with high DGP to 16% in London, 23% in Brindisi and 12% in Aswan. In all the cases, PV glasses reported similar – or even better – performances respect to SC

glasses. We found that the annual energy production attainable with BIPVs could be as high as the annual electric lighting energy consumption. In some cases, like Aswan and Brindisi, using large windows, the annual energy production even overcame the amount of electric energy used for artificial lighting. We also considered the effect of cell temperature on the performance of BIPV glazings, suitably correcting the conversion efficiency, according to experimental results: no variations appeared in locations with colder climate, whereas a maximum reduction of 3% was observed in hot desert climates.

Taking into account the whole set of results, it can be concluded that perovskite-based semitransparent PVs can indeed be considered a relevant technological opportunity to overcome the persisting barriers (mainly functional, economic and aesthetic) to a widespread diffusion of BIPVs. The manifold advantages deriving from the adoption of these PV films have been demonstrated and precisely estimated in terms of annual energy production, similar to those achieved with a-Si solar modules and in terms of visual comfort effects, demonstrating that this novel technology can be a reliable candidate for architectural uses.

Acknowledgments

A.C. kindly acknowledges Praveen Pattathil, from Istituto Italiano di Tecnologia (CBN-UniLe) for technical support. This activity was partially funded by the Action Co-founded by Cohesion and Development Fund 2007-2013 – APQ Research Puglia Region "Regional programme supporting smart specialization and social and environmental sustainability – FutureInResearch".

Appendix

The PV cell temperature may play a significant role in affecting its efficiency and, consequently, the overall energy yield. In order to take into account this contribution several approaches can be followed involving relatively simple models, based on a limited number of either environmental parameters (such as the Nominal Operative Cell Temperature (NOCT) approach [47] or the Sandia National Laboratory method [48], or cell specific parameters (such as the Equivalent Cell Temperature method [49]). Even though such approaches proved to yield sufficiently accurate results when referred to BIPV systems [50,51] , they have been defined for rack-mounted PV panels. As for

windows the overall heat exchange can be quite different, in the present case it seems more appropriate to use a more detailed heat balance model.

The calculation of the PV glass temperature was carried out assuming that, due to the large surface to volume ratio of a typical window glass combined with its negligible thickness, the (average) temperature of the pane can be considered to be a function of time only. Thus, the temperature variation of the cell during a time interval Δt was calculated as a function of the overall heat transfer entering the body during Δt. Within a finite difference framework, the new temperature at time t+Δt was calculated using the following equation:

$$T_{t+\Delta t} = T_t + \frac{\dot{Q}\Delta t}{\rho c \Delta x} \quad \text{(A.1)}$$

Where $\dot{Q}$ is the net heat power entering the glass pane [W/m^2], ρ is the glass density [kg/m^3], c is the specific heat [J/(kg·K)], and Δx is the pane thickness [m]. In order to have an accurate estimate of the temperature variations, a 5 minute interval was considered, requiring an interpolation of the weather data given in the dataset. The net heat power was calculated assuming that both faces of the glass pane exchanged heat by radiation and convection. The interior face was supposed to exchange heat with an isothermal cavity behaving as a black-body and filled with air at a temperature equal to 20°C during Fall and Winter and equal to 25°C during Spring and Summer. This temperature set-point was somewhat rough but, in order to compare different locations with different climatic profiles, a simple approach was preferable. Convective coefficient for the inside face of the pane was calculated as a function of the temperature difference between surface and air, according to the relationship given by ASHRAE [52] :

$$h_n = 1.31|\Delta T|^{1/3} \ \text{[W/m}^2\text{K]} \quad \text{(A.2)}$$

Convective coefficient for the outdoor surface was calculated as the sum of a natural convection term (calculated according to Eq. A.2), and a forced convection term, calculated according to Sparrow at al. [53] as:

$$h_f = 2.537 W_f \left(\frac{PV_z}{A}\right)^{1/2} \ \text{[W/m}^2\text{K]} \quad \text{(A.3)}$$

Where W_f is a coefficient equal to 1.0 for windward surfaces and to 0.5 for leeward surfaces, P is the surface perimeter [m], A is the surface area [m^2], and V_z is the local wind speed [m/s]. Finally radiative heat was divided between shortwave and longwave fractions. The first was assessed by multiplying the global radiation calculated as explained above by the solar absorptivity (α_s) which for the PV glass under investigation was assumed to be 0.5, considering that the measured visible transmittance is 0.42 and reflectance ranges between 0.04 and 0.08 for clear and gray glasses (as can be observed in EnergyPlus library of glass materials). The outdoor longwave radiation was calculated as a function of the sky temperature (retrieved from the weather dataset), the view factor, and the surface emissivity. The latter was measured using the indirect approach proposed by Avdelidis et al. [54] and was 0.83, in good agreement with typical values for clear and gray glasses. The same value was also used to compute the indoor longwave radiation exchange.

References

[1] Saifullah M, Gwak J, Yun JH. Comprehensive review on material requirements, present status, and future prospects for building-integrated semitransparent photovoltaics (BISTPV). J Mater Chem A 2016;4:8512–40. doi:10.1039/C6TA01016D.

[2] Gao T, Jelle BP, Ihara T, Gustavsen A. Insulating glazing units with silica aerogel granules: The impact of particle size. Appl Energy 2014;128:27–34. doi:10.1016/j.apenergy.2014.04.037.

[3] Jelle BP, Breivik C. The path to the building integrated photovoltaics of tomorrow. Energy Procedia 2012;20:78–87. doi:10.1016/j.egypro.2012.03.010.

[4] Akinyele DO, Rayudu RK, Nair NKC. Global progress in photovoltaic technologies and the scenario of development of solar panel plant and module performance estimation - Application in Nigeria. Renew Sustain Energy Rev 2015;48:112–39. doi:10.1016/j.rser.2015.03.021.

[5] Heinstein P, Ballif C, Perret-Aebi LE. Building integrated photovoltaics (BIPV): Review, potentials, barriers and myths. Green 2013;3:125–56. doi:10.1515/green-2013-0020.

[6] Benemann J, Chehab O, Schaar-gabriel E. Building-integrated PV modules 2001;67:345–54.

[7] Carlson DE, Wronski CR. Amorphous silicon solar cell Amorphous silicon solar cell 1976;671:1–4. doi:10.1063/1.88617.

[8] Martin A. Green, Keith Emery, Yoshihiro Hishikawa WW and EDD. Solar cell efficiency tables (Version 45). Prog Photovolt Res Appl 2015;23:1–9. doi:10.1002/pip.

[9] Song Z, Phillips AB, Krantz PW, Khanal RR, Heben MJ. Spray pyrolysis of semi-transparent backwall superstrate CuIn(S,Se)2 solar cells. 2014 IEEE 40th Photovolt Spec Conf PVSC 2014 2014:1712–7. doi:10.1109/PVSC.2014.6925251.

[10] Emmott CJM, Urbina A, Nelson J. Environmental and economic assessment of ITO-free electrodes for organic solar cells. Sol Energy Mater Sol Cells 2012;97:14–21. doi:10.1016/j.solmat.2011.09.024.

[11] Tan H, Furlan A, Li W, Arapov K, Santbergen R, Wienk MM, et al. Highly Efficient Hybrid Polymer and Amorphous Silicon Multijunction Solar Cells with Effective Optical Management. Adv Mater 2016;28:2170–7. doi:10.1002/adma.201504483.

[12] O'Regan B, Grätzel M. A low-cost, high-efficiency solar cell based on dye-sensitized colloidal TiO2 films. Nature 1991;353:737–9.

[13] Green M a., Ho-Baillie a., Snaith HJ. The emergence of perovskite solar cells. Nat Photonics 2014;8:506–14. doi:10.1038/nphoton.2014.134.

[14] Yang K, Li F, Zhang J, Veeramalai CP, Guo T. All-solution processed semi-transparent perovskite solar cells with silver nanowires electrode. Nanotechnology 2016;27:95202. doi:10.1088/0957-4484/27/9/095202.

[15] Zhang W, Anaya M, Lozano G, Calvo ME, Johnston MB, Miguez H, et al. Highly Efficient Perovskite Solar Cells with Tuneable Structural Color. Nano Lett 2015.

[16] Eperon GE, Stranks SD, Menelaou C, Johnston MB, Herz LM, Snaith HJ. Formamidinium lead trihalide: a broadly tunable perovskite for efficient planar heterojunction solar cells. Energy Environ Sci 2014;7:982. doi:10.1039/c3ee43822h.

[17] Cannavale A, Eperon GE, Cossari P, Abate A, Snaith HJ, Gigli G. Perovskite photovoltachromic cells for building integration. Energy Environ Sci 2015;8:1578–84.

[18] Gaspera E Della, Peng Y, Hou Q, Spiccia L, Bach U, Jasieniak JJ, et al. Ultra-thin High efficiency semitransparent perovskite solar cells. Nano Energy 2015;13:249–57. doi:10.1016/j.nanoen.2015.02.028.

[19] Eperon GE, Burlakov VM, Goriely A, Snaith HJ. Neutral color semitransparent microstructured perovskite solar cells. ACS Nano 2014;8:591–8. doi:10.1021/nn4052309.

[20] Hörantner MT, Nayak PK, Mukhopadhyay S, Wojciechowski K, Beck C, McMeekin D, et al. Shunt-Blocking Layers for Semitransparent Perovskite Solar Cells. Adv Mater Interfaces 2016:n/a-n/a. doi:10.1002/admi.201500837.

[21] Boyce P, Eklund N, Mangum S, Saalfield C, Tang L. Minimum acceptable

transmittance of glazing. Light Res Technol 1995;27:145–52. doi:10.1177/14771535950270030201.

[22] Clarissa Zomer, André Nobre, Pablo Cassatella TR and RR. The balance between aesthetics and performance in building-integrated photovoltaics in the tropics. Prog Photovolt Res Appl 2007;15:659–76. doi:10.1002/pip.

[23] Yang RJ, Zou PXW. Building integrated photovoltaics (BIPV): Costs, benefits, risks, barriers and improvement strategy. Int J Constr Manag 2016;16:39–53. doi:10.1080/15623599.2015.1117709.

[24] Chae YT, Kim J, Park H, Shin B. Building energy performance evaluation of building integrated photovoltaic (BIPV) window with semi-transparent solar cells. Appl Energy 2014;129:217–27. doi:10.1016/j.apenergy.2014.04.106.

[25] Oliver M, Jackson T. Energy and economic evaluation of building-integrated photovoltaics 2001;26:431–9.

[26] Cannavale A, Cossari P, Eperon GE, Colella S, Fiorito F, Gigli G, et al. Forthcoming Perspectives of Photoelectrochromic Devices: A critical review. Energy Environ Sci 2016;9:2682–719. doi:10.1039/C6EE01514J.

[27] Cannavale A, Fiorito F, Resta D, Gigli G. Visual comfort assessment of smart photovoltachromic windows. Energy Build 2013;65:137–45. doi:10.1016/j.enbuild.2013.06.019.

[28] Favoino F, Fiorito F, Cannavale A, Ranzi G, Overend M. Optimal control and performance of photovoltachromic switchable glazing for building integration in temperate climates. Appl Energy 2016;178:943–61. doi:10.1016/j.apenergy.2016.06.107.

[29] DeForest N, Shehabi A, O'Donnell J, Garcia G, Greenblatt J, Lee ES, et al. United States energy and CO2 savings potential from deployment of near-infrared electrochromic window glazings. Build Environ 2015;89:107–17. doi:10.1016/j.buildenv.2015.02.021.

[30] DeForest N, Shehabi A, Garcia G, Greenblatt J, Masanet E, Lee ES, et al. Regional performance targets for transparent near-infrared switching electrochromic window glazings. Build Environ 2013;61:160–8. doi:10.1016/j.buildenv.2012.12.004.

[31] Yoon S, Tak S, Kim J, Jun Y, Kang K, Park J. Application of transparent dye-sensitized solar cells to building integrated photovoltaic systems. Build Environ 2011;46:1899–904. doi:10.1016/j.buildenv.2011.03.010.

[32] ASHRAE. International Weather for Energy Calculations (IWEC Weather Files) Users Manual and CD-ROM. Atlanta: ASHRAE; 2001.

[33] Energy UD of. EnergyPlus version 8.6 documentation, Engineering Reference. 2016.

[34] R. Perez, P. Ineichen, R. Seals, J. Michalsky RS. Modeling daylight availability and irradiance components from direct and global irradiance. Sol Energy 1990;44:271–89. doi:10.1016/0038-092X(90)90055-H.

[35] M.C. Peel, B. L. Finlayson TAM. World map of the Köppen-Geiger climate classification updated. Hydrol Earth Syst Sci 2007;11:1633–44. doi:10.1127/0941-2948/2006/0130.

[36] Reinhart CF, Walkenhorst O. Validation of dynamic RADIANCE-based daylight simulations for a test office with external blinds. Energy Build 2001;33:683–97. doi:10.1016/S0378-7788(01)00058-5.

[37] Bourgeois D, Reinhart CF, Ward G. Standard daylight coefficient model for dynamic daylighting simulations. Build Res Inf 2008;36:68–82. doi:10.1080/09613210701446325.

[38] Favoino F, Overend M, Jin Q. The optimal thermo-optical properties and energy saving potential of adaptive glazing technologies. Appl Energy 2015;156:1–15. doi:http://dx.doi.org/10.1016/j.apenergy.2015.05.065.

[39] Nabil A, Mardaljevic J. Useful daylight illuminance: a new paradigm for assessing daylight in buildings. Light Res Technol 2005;37:41–59. doi:10.1191/1365782805li128oa.

[40] Nabil A, Mardaljevic J. Useful daylight illuminances: A replacement for daylight factors. Energy Build 2006;38:905–13. doi:10.1016/j.enbuild.2006.03.013.

[41] Wienold J, Christoffersen J. Evaluation methods and development of a new glare prediction model for daylight environments with the use of CCD cameras. Energy Build 2006;38:743–57. doi:10.1016/j.enbuild.2006.03.017.

[42] Mardaljevic J, Andersen M, Roy N, Christoffersen J. Daylighting Metrics: Is There a Relation Between Useful Daylight Illuminance and Daylight Glare Probability? Ibpsa-Engl Bso12 2012:189–96.

[43] Mardaljievic J. Validation of a lighting simulation program under real sky conditions. Light §res Technol 1995;27:181–8.

[44] Peng J, Curcija DC, Lu L, Selkowitz SE, Yang H, Zhang W. Numerical investigation of the energy saving potential of a semi-transparent photovoltaic double-skin facade in a cool-summer Mediterranean climate. Appl Energy 2016;165:345–56. doi:10.1016/j.apenergy.2015.12.074.

[45] Zhang W, Lu L, Peng J, Song A. Comparison of the overall energy performance of semi-transparent photovoltaic windows and common energy-efficient windows in Hong Kong. Energy Build 2016;128:511–8. doi:10.1016/j.enbuild.2016.07.016.

[46] Randall JF, Jacot J. Is AM1.5 applicable in practice? Modelling eight photovoltaic materials with respect to light intensity and two spectra. Renew Energy 2003;28:1851–64. doi:10.1016/S0960-1481(03)00068-5.

[47] Alonso García MC, Balenzategui JL. Estimation of photovoltaic module yearly temperature and performance based on Nominal Operation Cell Temperature calculations. Renew Energy 2004;29:1997–2010. doi:10.1016/j.renene.2004.03.010.

[48] King DL, Boyson WE, Kratochvil JA. Photovoltaic array performance model.

Sandia Rep No 2004-3535 2004;8:1–19. doi:10.2172/919131.

[49] 60904-5 I. Determination of the equivalent cell temperature (ECT) of photovoltaic (PV) devices by the open-circuit voltage method. 2nd ed. 2011.

[50] Chatzipanagi A, Frontini F, Virtuani A. BIPV-temp: A demonstrative Building Integrated Photovoltaic installation. Appl Energy 2016;173:1–12. doi:10.1016/j.apenergy.2016.03.097.

[51] Trinuruk P, Sorapipatana C, Chenvidhya D. Estimating operating cell temperature of BIPV modules in Thailand. Renew Energy 2009;34:2515–23. doi:10.1016/j.renene.2009.02.027.

[52] ASHRAE. ASHRAE Handbook - The fundamentals. Atlanta: American Society of Heating, Refrigerating and Air-Conditioning Engineers, Inc.; 2005.

[53] E. M. Sparrow JWR and EAM. Effect of Finite Width on Heat Transfer and Fluid Flow about an Inclined Rectangular Plate. J Heat Transf 1979;101:199–204.

[54] Avdelidis NP, Moropoulou A. Emissivity considerations in building thermography. Energy Build 2003;35:663–7. doi:10.1016/S0378-7788(02)00210-4.